Mapping Mediterranean Altimeter Data with a Multiresolution Optimal Interpolation Algorithm

P. Fieguth[1], D. Menemenlis[2], T. Ho[3], A. Willsky[3], and C. Wunsch[2]

last revision: May 25, 1997

Short title: MAPPING MEDITERRANEAN ALTIMETER DATA

[1]Department of Systems Design Engineering, University of Waterloo

[2]Department of Earth, Atmospheric, and Planetary Sciences, Massachusetts Institute of Technology

[3]Department of Electrical Engineering and Computer Science, Massachusetts Institute of Technology

Abstract.

A multiresolution optimal interpolation scheme is described and used to map the sea level anomaly of the Mediterranean Sea based on TOPEX/POSEIDON and ERS-1 data. The principal advantages of the multiresolution scheme are its high computational efficiency, the requirement for explicit statistical models for the oceanographic signal and the measurement errors, and the production of error variances for all estimates at multiple scales. A set of MATLAB-callable routines which implement the multiresolution scheme have been made available on FTP anonymous.

The oceanographic signal is here modeled as a stationary $1/k^{\mu}$ process, where k is the horizontal wavenumber. Measurement noise is modeled as the sum of two separate random processes: a Gaussian white noise process, and a correlated process of low wavenumber representing the uncertainties in the orbital position of the satellite and in the atmospheric load corrections. The efficiency of the multiresolution scheme allowed the testing of more than 16,000 sets of hypothesized statistical prior model parameters in order to determine the most likely parameters. Mapping results with and without low-wavenumber error corrections are presented and compared.

1. Introduction

The use of satellite altimeter data to study the circulation of the Mediterranean Sea is complicated by a poor signal-to-noise ratio [*Larnicol et al.*, 1995]: the sea level anomaly signal is at most 10 cm RMS in the energetic regions of the Mediterranean while the residual altimeter noise, including orbit and atmospheric load errors, is of order 5 cm RMS or more. By construction the sea level anomaly signal, which is here obtained by removing a four-year temporal mean at every point, does not contain any geoid errors, except for those due to lateral orbit errors over steep topography. The major sources of low wavenumber uncertainty are the orbit errors [*Marshall et al.*, 1995] and, in the Mediterranean, the atmospheric loading not removed by the inverse barometer correction [*Candela and Lozano*, 1994; *Le Traon and Gauzelin*, 1997]. Orbit and atmospheric loading errors are removed in practice, along with some of the oceanic signal, by fitting and subtracting low order polynomials or cubic splines from each altimeter track so as to minimize track-to-track crossover differences [*Le Traon et al.*, 1995b; *Larnicol et al.*, 1995; *Bonnefond et al.*, 1995; *Vasquez-Cuervo et al.*, 1996]. The problem with these methods is that they do not make use of an explicit statistical model for the low wavenumber errors: the crossover difference minimization algorithms are ad hoc, and the estimation of sea-surface topography and of orbit/atmospheric load corrections are treated as two separate steps, i.e., the uncertainties in the orbit correction step are not taken into account when estimating the sea surface topography.

In this paper, we use a multiresolution optimal interpolation scheme to map the sea level anomaly of the Mediterranean Sea based on TOPEX/POSEIDON and ERS-1 data. The departure of our work from previous efforts is that we *jointly* estimate the sea level anomaly and the orbit/atmospheric load errors, so that the uncertainties in the errors are naturally reflected in the estimates and vice versa. This approach requires explicit statistical models for the sea level anomaly and for the orbit and atmospheric load errors, and in turn provides estimation error variances for all estimates at multiple scales. The

major advantage of the multiresolution scheme is that its numerical implementation is extremely efficient, and therefore the estimation can be repeated a large number of times in order to test different statistical models and to obtain consistent results.

The multiresolution optimal interpolation scheme has previously been described and used for mapping altimeter data in the North Pacific Ocean by *Fieguth et al.* [1995], but is here substantially modified to allow for the joint estimation of orbit and atmospheric loading errors. The scheme is based on a scale-recursive statistical description of the processes under study. This particular statistical description permits the use of recursive estimation algorithms which provide a significant speed advantage over more conventional estimation algorithms. One difficulty associated with the implementation of such multiresolution optimal interpolation schemes is in the construction and specification of the multiscale statistical models. For this reason we are making our algorithm available on the Internet in the form of a Matlab callable routine (see Appendix A). In a related paper, *Menemenlis et al.* [1997a] describe a multiscale statistical model which can be applied to a more general class of estimation problems (again, with an algorithm available on the Internet).

2. Statistical Modeling

An abstract statistical description of the TOPEX/POSEIDON or ERS-1 altimeter data may be written as follows:

$$\text{Measurement equation:} \qquad h(t) = \zeta(x,y,t) + v(t) \tag{1}$$

$$\text{Sea surface prior covariance:} \qquad P(x,\bar{x},y,\bar{y},t,\bar{t}) = \langle \zeta(x,y,t) \cdot \zeta(\bar{x},\bar{y},\bar{t}) \rangle \tag{2}$$

$$\text{Measurement error covariance:} \qquad R(t,\bar{t}) = \langle v(t) \cdot v(\bar{t}) \rangle \,, \tag{3}$$

where $\zeta(x,y,t)$ represents the oceanographic sea level anomaly signal taken at time t and location $(x,\ y)$, and $h(t)$ represents the altimetric measurement of $\zeta(x,y,t)$ subject to noise $v(t)$ which includes residual tidal, atmospheric, and orbit errors. The

sea-surface height ζ and the measurement noise v are modeled to be zero mean (i.e., systematic signal components are assumed to have been removed), so that $\langle v(t) \rangle = 0$, $\langle \zeta(x,y,t) \rangle = 0$. $R(t,\bar{t})$ and $P(x,\bar{x},y,\bar{y},t,\bar{t})$ represent the second order prior statistics of $v(t)$ and $\zeta(x,y,t)$, respectively. Solving for the time-varying process $\zeta(x,y,t)$ based on the prior statistics and measurements in (1)–(3) is extremely difficult, predominantly due to the complicated ocean surface dynamics captured by $P(x,\bar{x},y,\bar{y},t,\bar{t})$. Instead, for the purposes of this paper, we consider the ocean surface to be static (a reasonable assumption for the large-scale, baroclinic modes of variability over periods up to ten days in length) and statistically stationary:

$$\langle \zeta(x,y,t) \cdot \zeta(\bar{x},\bar{y},\bar{t}) \rangle = P(x-\bar{x}, y-\bar{y}). \tag{4}$$

Motivated by spectral analyses of the altimetric data and earlier work [*Wunsch and Stammer*, 1995; *Fieguth et al.*, 1995; *Gaspar and Wunsch*, 1989] we propose to model the surface $\zeta(x,y,t)$ as a $1/k^{\mu}$ process, where k is the horizontal wavenumber.

Studies [*Fu et al.*, 1994; *Le Traon et al.*, 1994, 1995b] of the measurement noise suggest that the TOPEX/POSEIDON or ERS-1 noise process $v(t)$ can be modeled as the sum of two separate random processes:

$$v(t) = v_{WGN}(t) + v_{CORR}(t). \tag{5}$$

On the one hand, the random measurement error of each altimeter has a very short correlation period and is here modeled by a Gaussian white noise process $v_{WGN}(t)$. On the other hand, the uncertainties in the orbital position of the satellite and in the atmospheric load correction are a correlated process of low wavenumber, represented here by $v_{CORR}(t)$. Earlier altimetric optimal interpolation efforts have either ignored v_{CORR} [*Fieguth et al.*, 1995] or tried to remove it via a preprocessing step [*Larnicol et al.*, 1995] — an approach requiring ad-hoc assumptions and which fails to take into account the posterior error statistics of the preprocessing step when estimating $\zeta(x,y,t)$.

Instead, we propose to use an estimation framework which is flexible enough to allow us to specify the noise model (5) explicitly. For relatively small geographic areas such as the Mediterranean, the low-wavenumber error may be modeled as a low-order polynomial, leading to the following noise model:

$$v(i,t) = v_{WGN}(t) + \sum_{j=0}^{J} \alpha_j(i) t^j, \tag{6}$$

where J represents the order of the polynomial correction, and $\alpha_j(i)$ represents the unknown jth order polynomial coefficient for satellite track i. We model the $\alpha_j(i)$ as being uncorrelated with each other and with v_{WGN}; that is, each track is modeled as having independent errors. Although the estimator is capable of polynomial corrections to arbitrary degree, we have chosen to apply first order, $J = 1$ (i.e., to estimate bias and tilt) corrections only, consistent with the low order corrections applied by previous authors (*Larnicol et al.* [1995] used $J = 0$, *Vasquez-Cuervo et al.* [1996] used $J = 1$) so as to minimize the attenuation of the low-wavenumber oceanographic signal. The next step is to specify prior statistics for (6) in the form of $\langle v_{WGN}(t)^2 \rangle$ and $\langle \alpha_j(i)^2 \rangle$, and this completes the statistical description of the estimation problem.

In principle, the optimal interpolation (minimum variance) solution for the above estimation problem could be obtained by matrix inversion. However the fields computed in Section 3 are 100×225 pixels in size and directly estimating such fields would require the inversion of a $22,500 \times 22,500$ matrix. In practice, such an approach is computationally infeasible, so we propose to use a recently developed multiscale estimation framework [*Chou et al.*, 1994; *Luettgen et al.*, 1994; *Fieguth et al.*, 1995] which is capable of solving very large estimation problems with a modest amount of computational effort. Specifically, this framework will be capable of *jointly* computing the sea surface and the orbit/atmospheric load errors, while still computing estimation error statistics. This computational advantage does not come for free: it can be a significant challenge to develop multiscale models which capture the desired statistics

and the remainder of this section will address this challenge. In particular, the correlated noise term in (5) and (6), which was ignored in the model of *Fieguth et al.* [1995], required a nontrivial effort to model.

The ocean surface of interest is modeled as the finest scale of a multiscale stochastic process $\mathbf{z}(s)$ defined on a quad-tree, i.e., a tree on which each node has four descendents (except those nodes on the finest scale). The process $\mathbf{z}(s)$ and its associated measurement process $\mathbf{h}(s)$ are modeled as

$$\begin{aligned} \mathbf{z}(s) &= \mathbf{A}(s)\mathbf{z}(s\bar{\gamma}) + \mathbf{B}(s)\mathbf{w}(s), \qquad \langle \mathbf{z}(0) \rangle = 0, \qquad \mathbf{P}(0) = \left\langle \mathbf{z}(0)\,\mathbf{z}^T(0) \right\rangle, \\ \mathbf{h}(s) &= \mathbf{C}(s)\mathbf{z}(s) + \mathbf{v}(s), \qquad \langle \mathbf{v}(s) \rangle = 0, \qquad \mathbf{R}(s) = \left\langle \mathbf{v}(s)\,\mathbf{v}^T(s) \right\rangle, \end{aligned} \tag{7}$$

where s indexes the nodes of the multiscale tree with $s = 0$ indicating the root-node of the tree, $s\bar{\gamma}$ represents the parent of node s, and $\mathbf{w}(s)$ is a white noise process; for our altimetric problem, measurements exist only at the finest scale of the tree. The multiscale state $\mathbf{z}(s)$ is made up of bias and tilt parameters for each track, along with a multiresolution process $\zeta(s)$ which represents the ocean surface $\zeta(x, y, t)$:

$$\mathbf{z}(s) = \left[\zeta(s) \;\; \alpha_0(1) \;\; \alpha_1(1) \;\; \ldots \;\; \alpha_0(M) \;\; \alpha_1(M)\right]^T, \tag{8}$$

where M counts the number of satellite tracks present in the measurements and where we have assumed that $J = 1$, i.e., a first-order polynomial correction for the low-wavenumber errors. As in *Fieguth et al.* [1995], $\zeta(s)$ is a multiresolution description of the sea surface height: on fine scales of the tree $\zeta(s)$ captures the local sea surface height and on coarse scales $\zeta(s)$ captures broad averages. (For reasons of efficiency our software uses a reduced order $\mathbf{z}(s)$. In particular only those $\alpha_j(i)$ corresponding to tracks which are measured by children of s need to be kept in $\mathbf{z}(s)$. However for clarity we shall retain the state definition of (8) throughout this paper).

Given this definition of the state, (8), three quantities must be specified to complete the multiscale model: (i) a prior covariance, $\mathbf{P}(0)$, at the root node of the tree consistent with $\langle \alpha_j(i)^2 \rangle$; (ii) a multiscale state model, $\mathbf{A}(s)$ and $\mathbf{B}(s)$, consistent with (8) and the

$1/k^\mu$ prior on $\zeta(s)$; and (iii) a multiscale measurement model, $\mathbf{C}(s)$ and $\mathbf{R}(s)$, consistent with (1), (6), and $\langle v_{WGN}(t)^2 \rangle$.

The prior model $\mathbf{P}(0)$ can be written

$$\mathbf{P}(0) = \mathrm{diag}\left(\left\langle \zeta(0)^2 \right\rangle \ \left\langle \alpha_0(1)^2 \right\rangle \ \left\langle \alpha_1(1)^2 \right\rangle \ \ldots \ \left\langle \alpha_1(M)^2 \right\rangle \right), \tag{9}$$

where $\langle \zeta(0)^2 \rangle$ describes the prior sea level anomaly variance at the coarsest scale of the multiresolution tree.

The model for $\mathbf{z}(s)$ due to the $\alpha_j(i)$ is simple: the coefficients $\alpha_j(i)$ are just copied unchanged from parent to child. For the sea surface $\zeta(s)$ we use the $1/k^\mu$ multiscale model of *Fieguth et al.* [1995]: the scale-to-scale variations in $\zeta(s)$ are random with exponentially decreasing variance. The resulting multiscale model is

$$\mathbf{A}(s) = \mathbf{I}, \tag{10}$$

$$\mathbf{B}(s) = \mathrm{diag}\left(B_\circ 2^{(1-\mu)m(s)/2} \ \ 0 \ \ 0 \ \ \ldots \ \ 0 \right), \tag{11}$$

where $m(s)$ denotes the scale of node s on the multiscale tree. A discussion regarding the particular choice of $B_\circ$, μ, and $\langle \zeta(0)^2 \rangle$ may be found in *Fieguth et al.* [1995].

Finally, we need to define multiscale measurements at the finest scale of the tree, consistent with (1) and (6):

$$\mathbf{C}(s)\mathbf{z}(s) \ = \ \begin{bmatrix} \zeta(x,y,t_1) + \alpha_0(i_1) + \alpha_1(i_1) \cdot (l(s) - 37^\circ) \\ \vdots \\ \zeta(x,y,t_N) + \alpha_0(i_N) + \alpha_1(i_N) \cdot (l(s) - 37^\circ) \end{bmatrix}, \tag{12}$$

where N is the total number of tracks, $i_1, \ldots, i_N$, which pass through the finest scale pixel corresponding to node s. The N measurements are taken at times $t_1, \ldots, t_N$, and $l(s)$ represents the latitude in degrees at which these measurements were taken. (The latitude, $l(s)$, relative to 37°N is used as a convenient surrogate for time, t, in (6); this replacement is possible because along each track the measurement latitude is a nearly linear function of the measurement time.) Furthermore,

$$\mathbf{R}(s) = \mathrm{diag}\left(\langle v_{WGN}(t_1)^2 \rangle \ \ \ldots \ \ \langle v_{WGN}(t_N)^2 \rangle \right), \tag{13}$$

where the value assumed by each $\langle v_{WGN}(t)^2 \rangle$ along the diagonal of $\mathbf{R}(s)$ depends upon the satellite which took the measurement. At this point the description of the multiscale model structure is complete, and it is this model which will be used to compute the experimental results in the next section.

3. Experimental Results

To illustrate the application of the multiresolution estimator described above, we have mapped sea level anomaly TOPEX/POSEIDON and ERS-1 data in the Mediterranean. TOPEX/POSEIDON data were processed and interpolated onto a fixed 6 km equidistant alongtrack grid by *King et al.* [1994]: they include the standard environmental, inverse barometer, and orbit error corrections. Tidal corrections are from the CSR3.0 [*Shum et al.*, 1996] model. ERS-1 data are from the files distributed by AVISO [*Le Traon et al.*, 1995a]. In addition to the standard environmental corrections, the AVISO data include corrections of the ERS-1 orbit errors based on a global minimization of TOPEX/POSEIDON–ERS-1 crossover differences [*Le Traon et al.*, 1995b]. (This ad hoc orbit correction is not necessary since the multiresolution estimation framework can accommodate different bias and tilt priors, $\langle \alpha_j(i)^2 \rangle$, for each altimeter track. Nevertheless, sufficient orbit/atmospheric load errors remain to demonstrate the power of the multiresolution estimator.) A four-year (one-year for the ERS-1 altimeter) mean sea level is computed and subtracted from the data in order to obtain sea level anomaly.

The following subsections compare and contrast sea level anomaly maps of the Mediterranean Sea produced using several different methods: a) simple interpolation, b) multiscale estimation without polynomial corrections as in [*Fieguth et al.*, 1995], c) multiscale estimation with first-order polynomial corrections as discussed in Section 2, and d) a suboptimal space-time optimal interpolation algorithm. Each map is computed from the measurements of one 10-day TOPEX/POSEIDON repeat cycle; in particular,

we used TOPEX data from repeat cycle 24 (May 9–19, 1993) which exhibited significant correlated measurement errors and visually demonstrates the removal of residual orbit/atmospheric load errors. Finally, we show results from a joint TOPEX/ERS-1 estimation.

In each case, the anomaly map is a grid of 100×225 estimates. The multiscale estimates are computed on a tree having 9 scales, which corresponds to a finest scale of 256×256 pixels in size; each pixel is square, 23km on a side. Our algorithm requires that the measurements be defined on the finest scale of the multiscale tree and therefore the data need to be repositioned by up to $\pm 1/2$ pixel width. For this reason the pixel size must be chosen sufficiently fine for this repositioning to be trivial. The associated map is then just a particular 100×225 pixel subset of the finest scale. Prior statistics were obtained empirically from TOPEX/POSEIDON repeat cycles 3 to 161 (October 1992 to February 1997) and from ERS-1 repeat cycles 6 to 18 (October 1992 to January 1994).

Prior Statistics

As mentioned earlier, the efficiency of the multiresolution estimator permits the testing of a large number of hypothesized statistical prior models. We conducted a series of tests to determine the most likely prior model parameters [*Luettgen and Willsky*, 1995; *Fieguth and Willsky*, 1996]. (In all, more than 16,000 tests, one test per hypothesized parameter setting, of the Mediterranean sea level anomaly were created to obtain the results summarized below; each test required about one tenth the computational effort of the estimates which follow.) Figure 1 displays the optimal value for the white measurement error variance, $\langle v_{WGN}(t)^2 \rangle$, for individual repeat cycles of each of the three altimeters. These values are determined by computing the statistical likelihood of the satellite data and the multiscale prior model for a variety of choices of $\langle v_{WGN}(t)^2 \rangle$; the optimal choice is the one corresponding to the greatest likelihood. The results are

Figure 1.

unambiguous: they suggest measurement noise standard deviation values of 3 cm, 6 cm, and 6.5 cm for the TOPEX, POSEIDON, and ERS-1 altimeters, respectively.

Figure 2 displays the results of jointly optimizing the model parameters B_o and μ in (11), based on the measurement noise values established for TOPEX in the previous paragraph. (The data are distributed along the exponential $B_o 2^{(1-\mu)\cdot 3}$ = constant, shown as a dashed line in Fig. 2. The distribution of points *away* from the dashed line reflects fine-scale statistical variability while the distribution *along* the line reflects coarse-scale variability. Essentially, the multiscale decomposition allows fine-scale statistics to be determined in great detail, whereas coarse-scale statistics are subject to larger uncertainty.) Despite this spread, Fig. 2 suggests that $B_o = 3.5$ cm and $\mu = 1.4$ constitute a reasonable choice as prior model parameters. Table 1 shows the results of a sensitivity test for this multiscale model: the estimates and error statistics are not particularly sensitive to the choice of model, varying by 3.5% and 4.4%, respectively, per 1 cm change in B_o and corresponding change in μ (about 0.15) along the dashed line plotted in Fig. 2.

Figure 2.

Table 1.

Figure 3 displays the optimal bias and tilt coefficient standard deviations, with the prior model and measurement noise parameters set as determined in the above two paragraphs. The most striking feature is the seasonal modulation of the optimized values. During the summer months, the bias is on the order of 2.5 cm, but it increases to 4–8 cm during the winter. This seasonal modulation is consistent with the hypothesis that the low-wavenumber error budget in the Mediterranean is dominated by relatively small orbit errors during the summer months and by larger atmospheric load and other environmental correction errors during the winter months when more and stronger storm systems move through the region. The tilt standard deviations demonstrate a similar, although less pronounced, variation, going from about 0.3 (cm/° latitude) in the summer months to about 0.7 (cm/° latitude) in the winter months. The actual bias and tilt statistics chosen will clearly depend on the repeat cycle being studied.

Figure 3.

Table 2 summarizes the prior statistics which we used in the multiscale processing of data from repeat cycle 24; the various results are described and contrasted in the following subsections. **Table 2.**

Basic Interpolation

Figure 4 displays the coverage of the TOPEX altimeter and a surface height anomaly map obtained using a simple interpolation scheme (an iterative FFT method [*Beer*, 1983, Section 12.3] has been applied to fill the gaps between the TOPEX altimeter data locations). This approach does not attempt to remove correlated measurement errors, nor does it produce any sort of estimation error statistics. **Figure 4.**

Multiscale — No Correlated Error Model

Figure 5 shows the surface height estimates and associated uncertainties based on a multiscale model as in *Fieguth et al.* [1995]: the multiscale model is identical to that described in Section 2 but does not take into account correlated measurement errors, i.e., $v(i,t) = v_{WGM}(t)$ in (6). The results are computed in 50 seconds on a Sun SPARC-10. **Figure 5.**

On scales in excess of 500 km, the multiscale estimates and those of the interpolated map in Fig. 4 are similar, however noticeable differences appear on shorter scales. In particular, the interpolated map suffers from a very large variability at fine scales; this variability is considerably ameliorated in the multiscale results of Fig. 5 because the prior model constrains the ocean surface estimates. However both maps suffer from obvious flaws in the vicinity of altimeter tracks due to low-wavenumber orbit and atmospheric load errors. In addition to the improved quality in the estimates, the point that distinguishes this multiscale model from the simple interpolation scheme is the ability to compute estimation error statistics. Qualitatively, the estimated uncertainty map in the bottom half of Fig. 4 is not surprising: the uncertainty is lowest near the satellite measurements and increases as one moves away.

Multiscale — Correlated Error Model

Figure 6 shows the surface height estimates and associated uncertainties based on the multiscale model of Section 2 which models the correlated component of the satellite measurement error as a first-order polynomial. The increase in the multiscale state dimension, i.e., the dimension of $\mathbf{z}(s)$ in (8), increases the computational requirements — 4 minutes on a Sun SPARC-10. **Figure 6.**

The difference between the correlated error model and its primitive cousin, presented in the previous subsection, becomes clear when comparing the estimates of Figs. 5 and 6. The obvious inconsistencies present in the estimates of Fig. 5 along the altimeter tracks have largely disappeared in Fig. 6. Indeed, whereas the dominant features in the estimates of Fig. 5 (and also of Fig. 4) are light and dark lines, each due to the correlated error of a single track, the estimates of Fig. 6 most prominently reveal broad regions of higher or lower sea surface elevation, with the satellite tracks appearing only as secondary features resulting from the higher accuracy (smaller uncertainty) of the estimates in the vicinity of the measurements.

In addition to the error statistics of the surface, shown in Fig. 6, it should be pointed out that the error statistics of the correlated measurement error are also computed, i.e., the error statistics of the coefficients $\alpha_j(i)$ in (6).

Suboptimal Space-Time Interpolation

The map and uncertainty estimates of Fig. 6 can also be compared and contrasted to those of Fig. 7 which were produced using suboptimal space-time interpolation [Nadia Ayoub and Pierre De Mey, personal communication 1996], and which are an example of maps that have been used to study Mediterranean circulation [*Ayoub et al.*, 1997]. The qualitative difference between the multiscale and the space-time interpolation maps results primarily from the use of different statistical priors. For the multiscale maps, the ocean is modeled as the $1/k^{\mu}$ process described earlier which makes allowance **Figure 7.**

for correlations at multiple scales. The space-time interpolation maps were obtained assuming a spatial decorrelation scale of 150 km and temporal decorrelation of 15 days. We have compared a series of maps for TOPEX/POSEIDON repeat cycles 2–75 created using the multiscale interpolation scheme with maps created using the space-time interpolation scheme. The conclusion is that both sets of maps are in general consistent to within the uncertainty of the multiscale estimates. The major difference between the two interpolation schemes lies in the estimates of uncertainty which are a very sensitive function of prior statistical assumptions. On the one hand, the decorrelation scales for the space-time interpolation scheme were chosen somewhat arbitrarily to produce reasonable-looking results. On the other hand, the computational efficiency of the multiscale estimates permitted a systematic search for a set of statistical parameters which are consistent with all of the available data. Realistic estimates of uncertainty are of primary importance for quantitative studies of the circulation and for blending the altimeter data with other observations or with model output.

Multiscale — Joint TOPEX/POSEIDON–ERS-1 Estimation

One final application will demonstrate the ability of our model to fuse TOPEX/-POSEIDON and ERS-1 data. Since the ERS-1 repeat cycle spans 35 days, only the subset of ERS-1 measurements falling within the 10 day period of TOPEX/POSEIDON repeat 24 were used. The additional coverage provided by the ERS-1 altimeter during that period is illustrated in Fig. 8. Fig. 9 shows the resulting estimates and error statistics, computed using the correlated measurement-error model of Section 2. The inclusion of the ERS-1 data introduces additional tracks, hence additional $\alpha_j(i)$ coefficients, hence a higher multiscale state dimension. Therefore estimates and error statistics are computed in about 5 minutes on a Sun SPARC-10, as compared to 4 minutes without the ERS-1 measurements. The addition of the ERS-1 data does not substantially modify the estimate of sea level anomaly. However the reduction in the

Figure 8.

Figure 9.

uncertainty is significant over most of the domain.

4. Concluding Remarks

Most of our past efforts [*Chou et al.*, 1994; *Luettgen et al.*, 1994; *Fieguth et al.*, 1995] with respect to the multiscale framework have concentrated on developing models and on understanding the statistical properties of the framework. We now believe that our understanding has improved to the point where our framework can make real scientific contributions and be used by other researchers as a tool for solving related estimation problems [*Menemenlis et al.*, 1997a, 1997b].

The particular mapping example discussed in this paper assumes a model on a square grid which is stationary, $1/k$-like, and static in time. The assumption of a stationary model on a square grid admittedly restricts this software to regional investigations, since at ocean basin scales the curvature of the earth is inconsistent with such a model. The use of a $1/f$-like prior model leads to a simple model in our multiscale framework; other prior models are possible [*Menemenlis et al.*, 1997a], but require more complicated multiscale implementations. Finally, the assumption that the ocean is static limits the time window of measurements to be used in producing a single map. However three aspects of the multiscale method lend themselves to processing dynamic data:

1. The computational efficiency of the framework makes it practical to compute large numbers of maps, successive in time, which could then be interpolated.

2. The present framework's tolerance for nonstationarities allows the definition of a time-varying measurement noise variance. For example, (13) can be modified such that the diagonal elements of $\mathbf{R}(s)$ take the form

$$\left\langle v_{WGN}(t_i)^2 \right\rangle + \phi(|t_i - t_o|) \tag{14}$$

where $\phi(|t_i - t_o|)$ is a positive, monotonically increasing function, and t_o is a given time origin. Such a definition of $\mathbf{R}(s)$ would have the effect of downweighting measurements which lie away from the time origin t_o [*Fieguth*, 1995].

3. In principle an oct-tree could be constructed — multiscale in two space dimensions and one in time. This would be a very elegant solution to the nonstationarity issue, however the development of efficient models on such trees presents formidable challenges and is the subject of ongoing research.

It must be pointed out, however, that the regional and time-stationary limitations are inherent in our particular chosen *model*, not in the multiscale framework itself. The development of nonstationary [*Fieguth et al.*, 1995; *Fieguth*, 1995] or temporally dynamic multiscale models is also the subject of ongoing research.

Appendix A: MATLAB-Callable Optimal Interpolation Code

The implementation of the multiscale estimation algorithm in its full generality is a rather complicated undertaking. In the interest of promoting the use of this algorithm and enabling interested researchers to apply it to problems of their own, we are making this code publicly available. The front-end visible to the user is written in MATLAB, and the multiscale computational engine is written in C. No programming experience is needed to try the software, although a significant understanding of MATLAB scripts would be required to customize our program for a different application.

Anyone interested in compiling and running our code will require MATLAB (4.x or higher) software and an ANSI-compatible C compiler (precompiled versions of the code, not requiring any compilation, are available for Sun-SPARC and SGI platforms). Most workstations should have ample computational power; all of our results were computed on a Sun-SPARC 10. However large multiscale trees require a large amount of memory, particularly for high state dimensions (i.e., for polynomial corrections of order $J > 1$,

or for problems with a very large number of satellite tracks). At least 50 Mbytes is required to run the programs for small test cases; 128 Mbytes or more is recommended for serious research applications.

The programs may be obtained via anonymous FTP to **lids.mit.edu** (IP Address 18.78.0.101) from directory **pub/ssg/code/Mediterranean**. The file README describes the purpose of each program and how to get started.

Acknowledgments. The authors thank Charmaine King for help with the processing of TOPEX/POSEIDON data, and Nadia Ayoub and Pierre De Mey for helpful discussions and for making available their sea level anomaly maps to compare with the multiscale estimates. Financial support was provided by ONR Grant N00014–91–J–1004, by ONR Grant N00014–93–1–1104, by contract 958125 from the Jet Propulsion Laboratory, and by SERDP/ARPA as part of the ATOC project (Univ. of California SIO contract PO#10037358).

References

Ayoub, N., P.-Y. Le Traon, and P. De Mey, A description of the Mediterranean surface variable circulation from combined ERS-1 and TOPEX/POSEIDON altimetric data, *J. Mar. Sys.*, in press, 1997.

Beer, T., *Environmental Oceanography: An Introduction to the Behaviour of Coastal Waters.* Pergamon, New York, 1983.

Bonnefond, P., P. Exertier, P. Schaeffer, S. Bruinsma, and F. Barlier, Satellite altimetry from a short-arc orbit technique: Application to the Mediterranean, *J. Geophys. Res.*, *100*(C12), 25,365–25,382, 1995.

Candela, J., and C. J. Lozano, Barotropic response of the western Mediterranean to observed atmospheric pressure forcing, in *The Seasonal and Interannual Variability of the Western Mediterranean Sea*, edited by P. La Violette, chap. 14, pp. 325–359. American Geophysical Union, Washington, D.C., 1994.

Chou, K., A. Willsky, and A. Benveniste, Multiscale recursive estimation, data fusion, and regularization, *IEEE Trans. Autom. Control*, *39*(3), 464–478, 1994.

Fieguth, P. W., Application of multiscale estimation to large scale multidimensional imaging and remote sensing problems, Ph.D. thesis, Massachusetts Institute of Technology, 1995.

Fieguth, P. W., and A. S. Willsky, Fractal estimation using models on multiscale trees, *IEEE Trans. Signal Processing*, *44*(5), 1297–1300, 1996.

Fieguth, P. W., W. C. Karl, A. S. Willsky, and C. Wunsch, Multiresolution optimal interpolation and statistical analysis of TOPEX/POSEIDON satellite altimetry, *IEEE Trans. Geosci. Remote Sens.*, *33*(2), 280–292, 1995.

Fu, L.-L., E. J. Christensen, C. A. Yamarone Jr., M. Lefebvre, Y. Ménard, M. Dorrer, and P. Escudier, TOPEX/POSEIDON mission overview, *J. Geophys. Res.*, *99*(C12), 24,369–24,381, 1994.

Gaspar, P., and C. Wunsch, Estimates from altimeter data of barotropic rossby waves in the northwestern Atlantic Ocean, *J. Phys. Oceanogr.*, *19*(12), 1821–1844, 1989.

King, C., D. Stammer, and C. Wunsch, The CMPO/MIT TOPEX/POSEIDON altimetric data set, Report 30, Massachusetts Institute of Technology, Cambridge, 1994.

Larnicol, G., P.-Y. Le Traon, N. Ayoub, and P. D. Mey, Mean sea level and surface circulation variability of the Mediterranean Sea from two years of TOPEX/POSEIDON altimetry, *J. Geophys. Res.*, *100*(C12), 25,163–25,177, 1995.

Le Traon, P.-Y., and P. Gauzelin, Response of the Mediterranean mean sea level to atmospheric pressure forcing, *J. Geophys. Res.*, *102*(C1), 973–984, 1997.

Le Traon, P.-Y., J. Stum, J. Dorandeau, and P. Gaspar, Global statistical analysis of TOPEX and POSEIDON data, *J. Geophys. Res.*, *99*(C12), 25,619–25,631, 1994.

Le Traon, P.-Y., F. Blanc, J. Dorandeau, P. Gaspar, P. Sicard, J. Stum, and P. Vincent, AVISO user handbook: Sea level anomaly files, Tech. Rep. AVI-NT-011-312-CN, Centre National d'Etudes Spatiales, Toulouse Cedex, France, 1995a.

Le Traon, P.-Y., P. Gaspar, F. Bouyssel, and H. Makhmara, Using Topex/Poseidon data to enhance ERS-1 data, *J. Atmos. Oceanic Technol.*, *12*, 161–170, 1995b.

Luettgen, M., and A. S. Willsky, Likelihood calculation for a class of multiscale stochastic models, with application to texture discrimination, *IEEE Trans. Image Processing*, *4*(2), 194–207, 1995.

Luettgen, M., W. Karl, and A. Willsky, Efficient multiscale regularization with applications to the computation of optical flow, *IEEE Trans. Image Processing*, *3*(1), 41–64, 1994.

Marshall, J. A., N. P. Zelensky, S. M. Klosko, D. S. Chinn, S. B. Luthcke, K. E. Rachlin, and R. G. Williamson, The temporal and spatial characteristics of TOPEX/POSEIDON radial orbit error, *J. Geophys. Res.*, *100*(C12), 25,331–25,352, 1995.

Menemenlis, D., T. Webb, C. Wunsch, U. Send, and C. Hill, Basin-scale ocean circulation from combined altimetric, tomographic and model data, *Nature*, *385*, 618–621, 1997b.

Menemenlis, D., P. W. Fieguth, C. Wunsch, and A. S. Willsky, Adaptation of a fast optimal interpolation algorithm to the mapping of oceanographic data, *J. Geophys. Res.*, in press, 1997a.

Shum, C. K., et al., Accuracy assessment of recent ocean tide models, *J. Geophys. Res.*, in press, 1996.

Vasquez-Cuervo, J., J. Font, and J. J. Martinez-Benjamin, Observations on the circulation in the alboran sea using ERS1 altimetry and sea surface temperature data, *J. Geophys. Res.*, in press, 1996.

Wunsch, C., and D. Stammer, The global frequency-wavenumber spectrum of oceanic variability estimated from TOPEX/POSEIDON altimetric measurements, *J. Geophys. Res.*, *100*(C12), 24,895–24,910, 1995.

Received _____

With the extension package 'AGU^{++}', version 1.2 from 1995/01/12

Figure Captions

Figure 1. Optimal standard deviation for the measurement noise of the TOPEX, POSEIDON, and ERS-1 altimeters.

Figure 2. Optimal oceanographic model parameters of the measured sea level anomaly signal for TOPEX data in repeat cycles 18 through 161. The horizontal axis plots B_o, the standard deviation of $\zeta(s)$ at the coarsest scale, and the vertical axis plots the spectral exponent, μ in (11). The dashed line plots $B_o 2^{(1-\mu)\cdot 3}$ = constant; the distribution of points *along* and *across* the curve reflect coarse-scale and fine-scale variability, respectively.

Figure 3. Optimal standard deviation of the bias and tilt coefficients, $(\alpha_0(i))$ and $(\alpha_1(i))$ in (6), for each TOPEX repeat cycle. The dashed lines show four-month averages.

Figure 4. Top: Mediterranean coverage of the TOPEX altimeter for the period May 9–19, 1993 (repeat cycle 24), with each data point gridded to the finest scale of the multiscale tree. Bottom: sea level anomaly map for this period created using a simple interpolation scheme. Contour intervals are 3 cm.

Figure 5. Multiscale estimates (top) and standard deviation of uncertainty (bottom) of sea level anomaly. The maps are based on the same 10-day TOPEX data as in Fig. 4, and they do not take correlated errors into account. Contour intervals of the estimates are 3 cm. Contour intervals of the error estimates are 0.5 cm with the 2 cm contour marked in bold.

Figure 6. Multiscale estimates (top) and standard deviation of uncertainty (bottom) of sea level anomaly. The maps are based on the same 10-day TOPEX data as in Figs. 4 and 5, but this time a first-order polynomial model has been used to remove the correlated component of measurement error along each satellite track. Contour intervals are as in Fig. 5.

Figure 7. Maps of sea-level anomaly (top) and normalised mapping error variance as a percentage of the total signal variance (bottom) for a sub-optimal space time optimal interpolation scheme. The maps are based on the same 10-day TOPEX data as in Figs. 4, 5, and 6. Contour intervals are 3 cm for the estimates and 20% for the uncertainty. (Courtesy of Nadia Ayoub and Pierre De May.)

Figure 8. Additional coverage provided by the ERS-1 altimeter for the period May 9–19, 1993 (repeat cycle 24), concurrent with that of Figs. 4, 5, 6, and 7. The small dots indicate tracks of the TOPEX altimeter while the larger dots indicate ERS-1 tracks; the dots are shown gridded to the finest scale of the multiscale tree.

Figure 9. Multiscale estimates (top) and standard deviation of uncertainty (bottom) of sea level anomaly. The maps are computed from TOPEX and ERS-1 data using the same multiscale model as that used to create Fig. 6. Contour intervals are as in Figs. 5 and 6.

Tables

Map	RMS of Estimate (cm)	RMS of Std. Error (cm)
Map 1: $B_o = 2.5,\ \mu = 1.24$	4.771	3.024
Map 2: $B_o = 3.5,\ \mu = 1.40$	4.932	3.142
Map 3: $B_o = 4.5,\ \mu = 1.53$	5.014	3.183
(Map 3 − Map 1)	0.344	0.277

Table 1. Sensitivity of the multiscale estimates and error statistics to the multiscale model parameters for TOPEX repeat cycle 24. These figures imply an estimate sensitivity of 3.5% and a standard error sensitivity of 4.4%, per unit of B_o.

TOPEX measurement noise variance, $\langle v_{WGN}(t)^2 \rangle$:	$(3 \text{ cm})^2$
ERS-1 measurement noise variance, $\langle v_{WGN}(t)^2 \rangle$:	$(6.5 \text{ cm})^2$
Bias variance, $\langle \alpha_0(i)^2 \rangle$:	$(4 \text{ cm})^2$
Tilt variance, $\langle \alpha_1(i)^2 \rangle$:	$(0.4 \text{ cm}/^\circ \text{ latitude})^2$
Spectral slope, μ, in $1/k^\mu$ model:	1.4
Coarse scale standard deviation, B_o:	3.5 cm
Mean sea level anomaly variance, $\langle \zeta(0)^2 \rangle$:	25 cm^2

Table 2. Prior model parameters for multiresolution estimates of TOPEX repeat cycle 24.

Figures

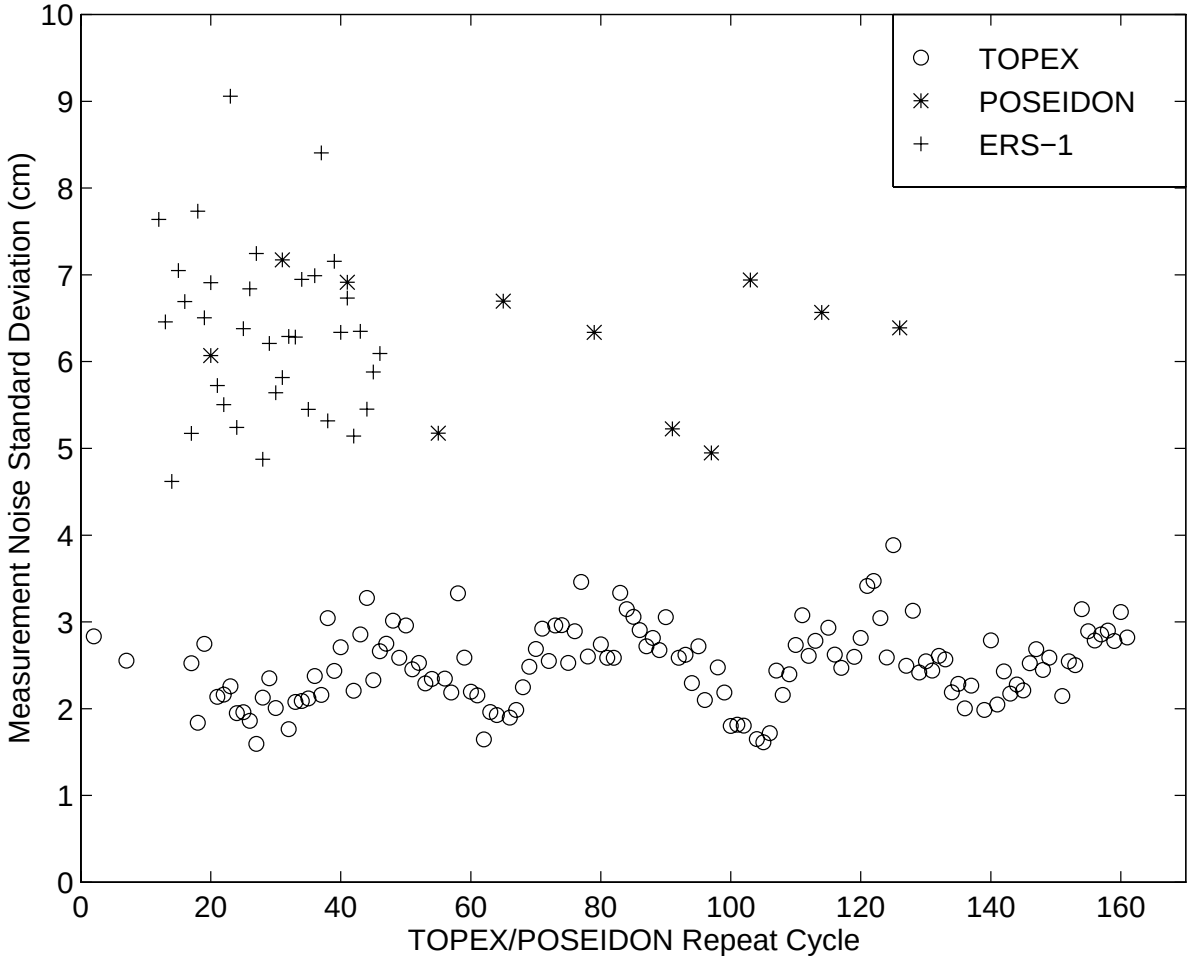

Figure 1. Optimal standard deviation for the measurement noise of the TOPEX, POSEIDON, and ERS-1 altimeters.

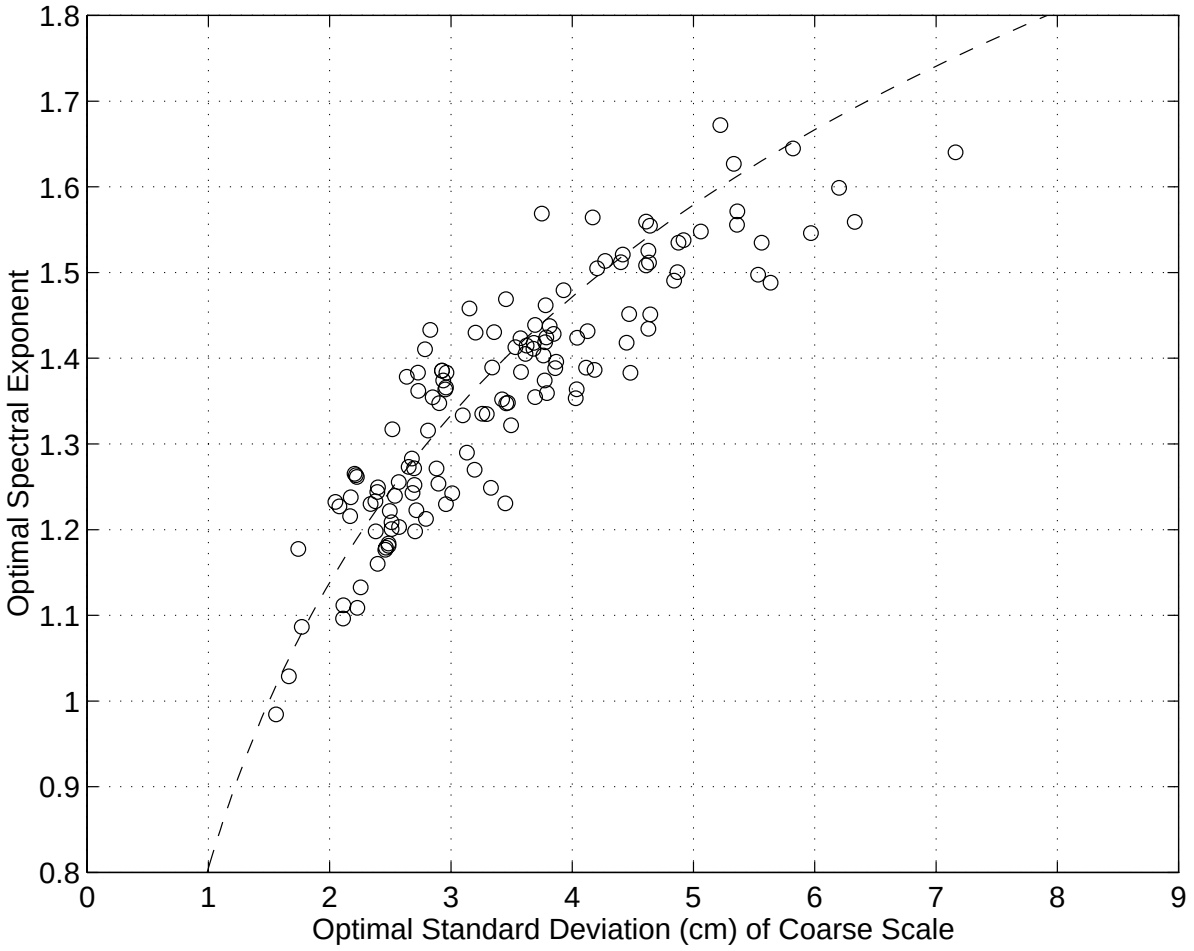

Figure 2. Optimal oceanographic model parameters of the measured sea level anomaly signal for TOPEX data in repeat cycles 18 through 161. The horizontal axis plots B_o, the standard deviation of $\zeta(s)$ at the coarsest scale, and the vertical axis plots the spectral exponent, μ in (11). The dashed line plots $B_o 2^{(1-\mu)\cdot 3}$ = constant; the distribution of points *along* and *across* the curve reflect coarse-scale and fine-scale variability, respectively.

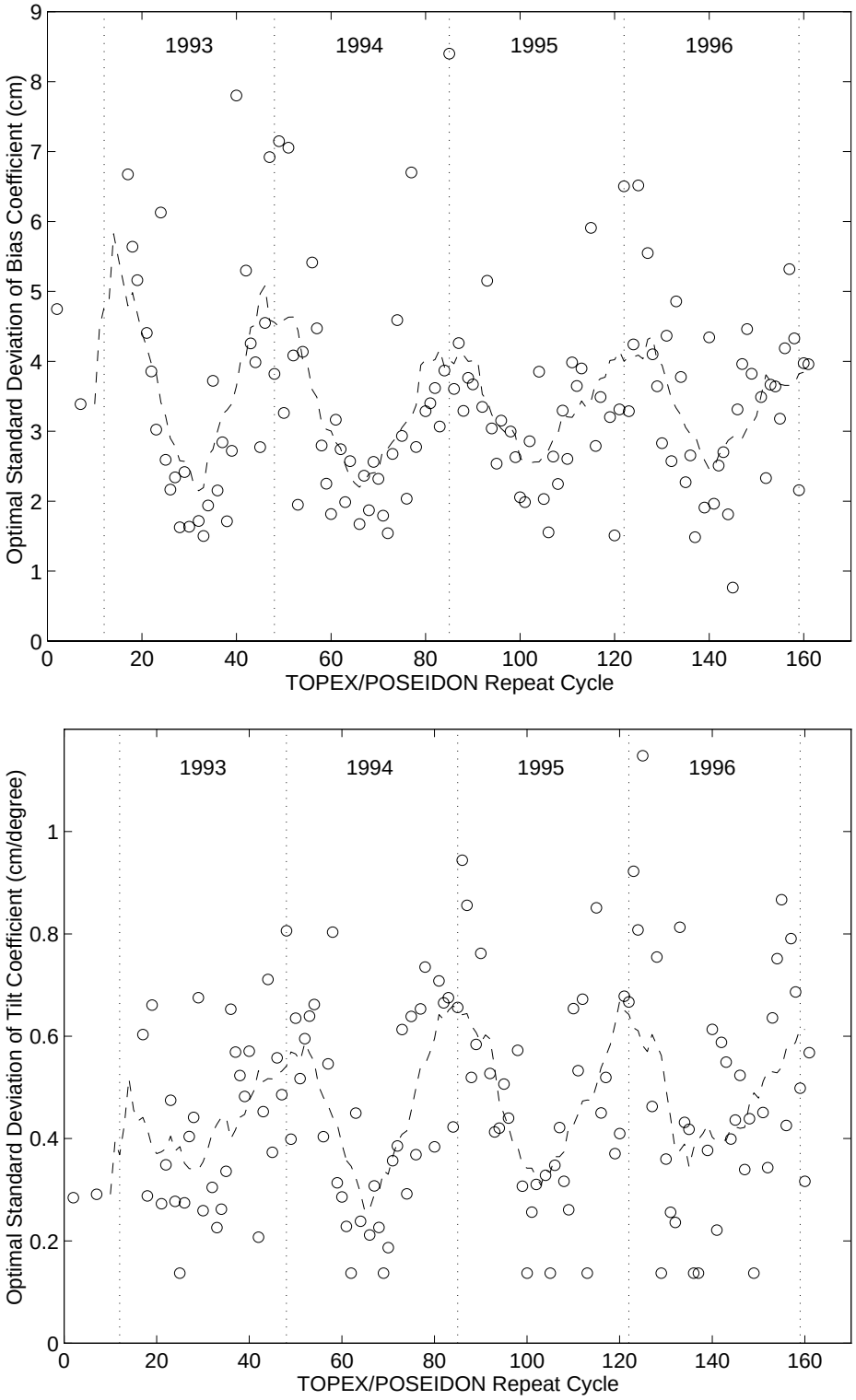

Figure 3. Optimal standard deviation of the bias and tilt coefficients, $(\alpha_0(i))$ and $(\alpha_1(i))$ in (6), for each TOPEX repeat cycle. The dashed lines show four-month averages.

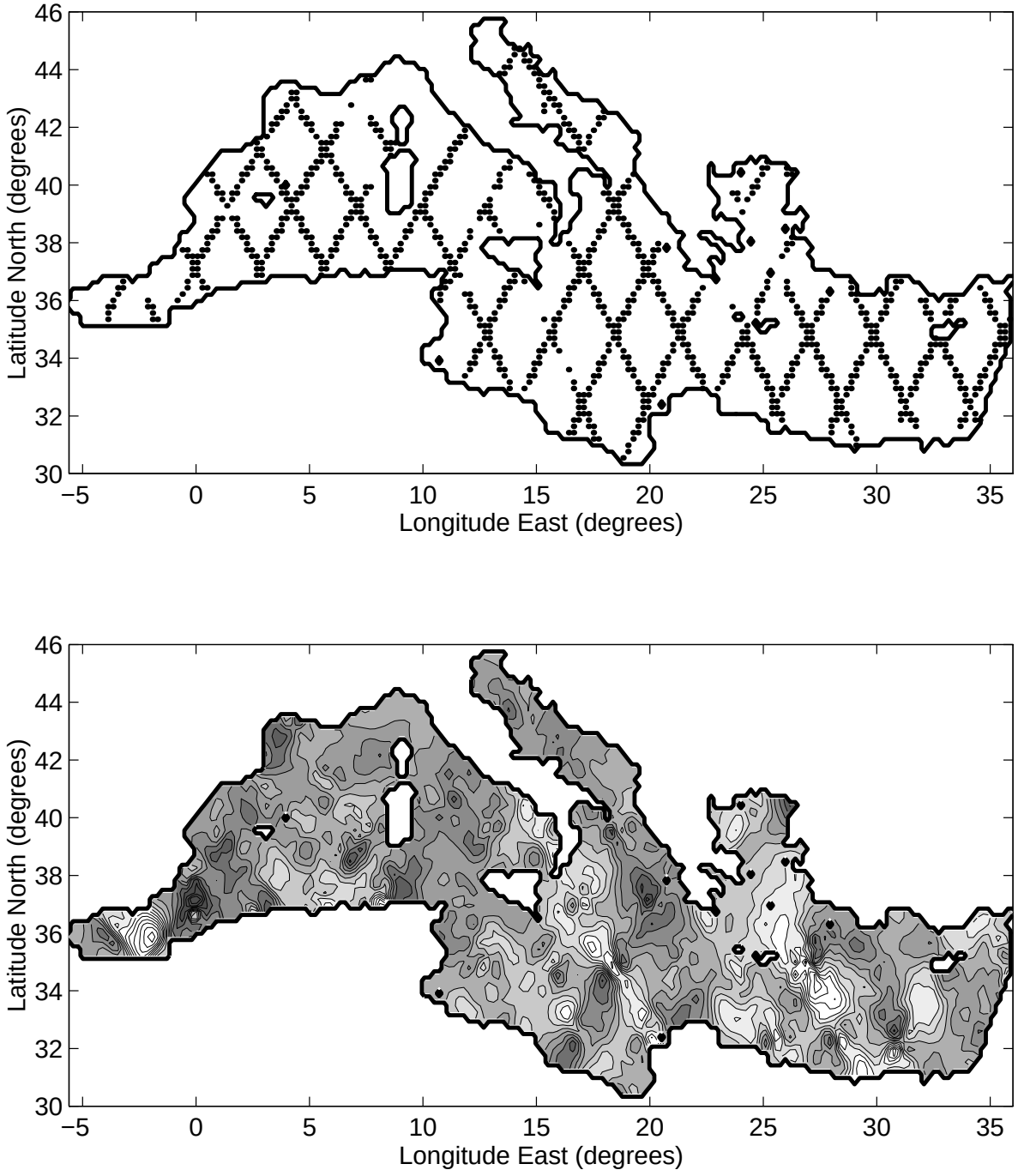

Figure 4. Top: Mediterranean coverage of the TOPEX altimeter for the period May 9–19, 1993 (repeat cycle 24), with each data point gridded to the finest scale of the multiscale tree. Bottom: sea level anomaly map for this period created using a simple interpolation scheme. Contour intervals are 3 cm.

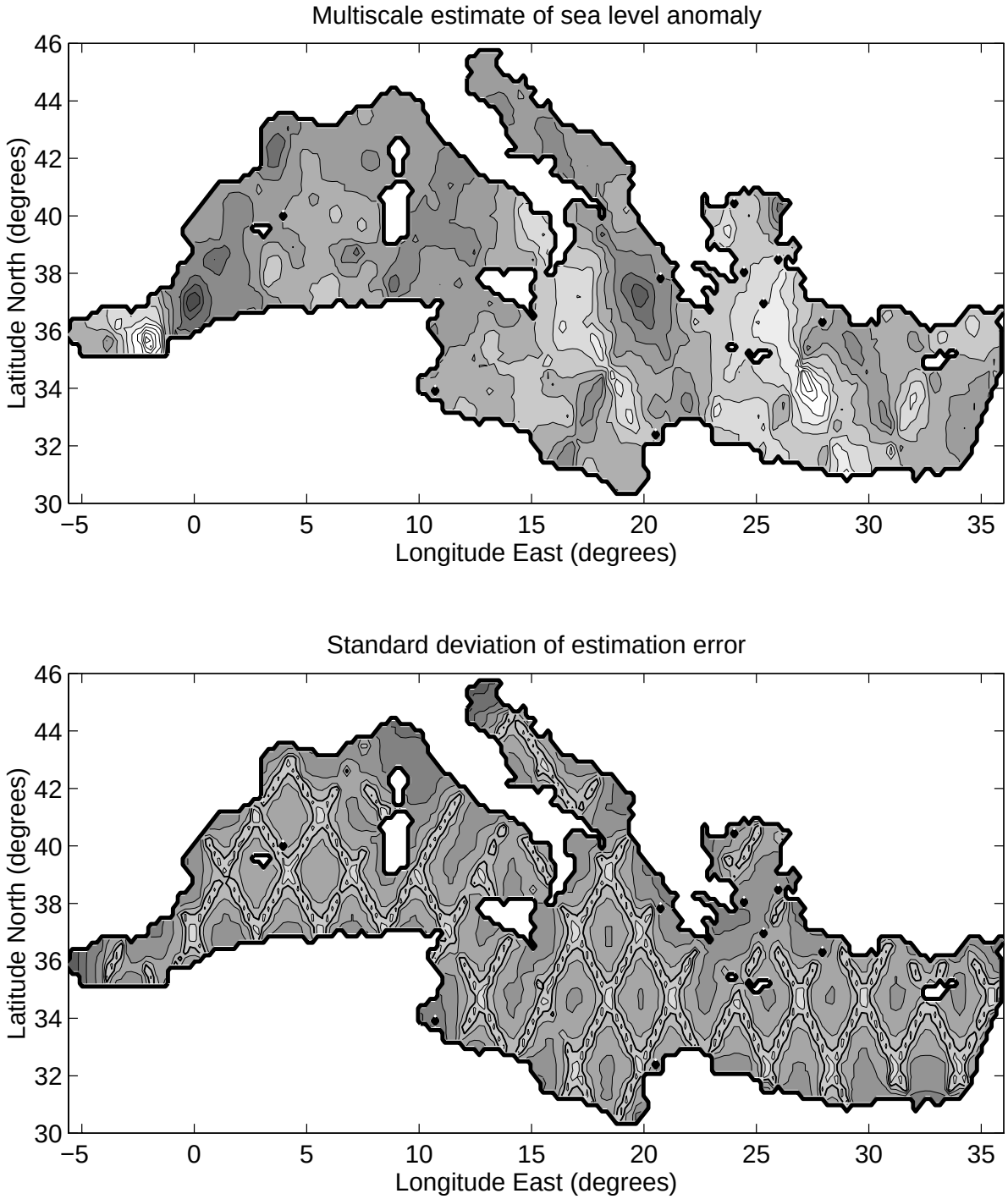

Figure 5. Multiscale estimates (top) and standard deviation of uncertainty (bottom) of sea level anomaly. The maps are based on the same 10-day TOPEX data as in Fig. 4, and they do not take correlated errors into account. Contour intervals of the estimates are 3 cm. Contour intervals of the error estimates are 0.5 cm with the 2 cm contour marked in bold.

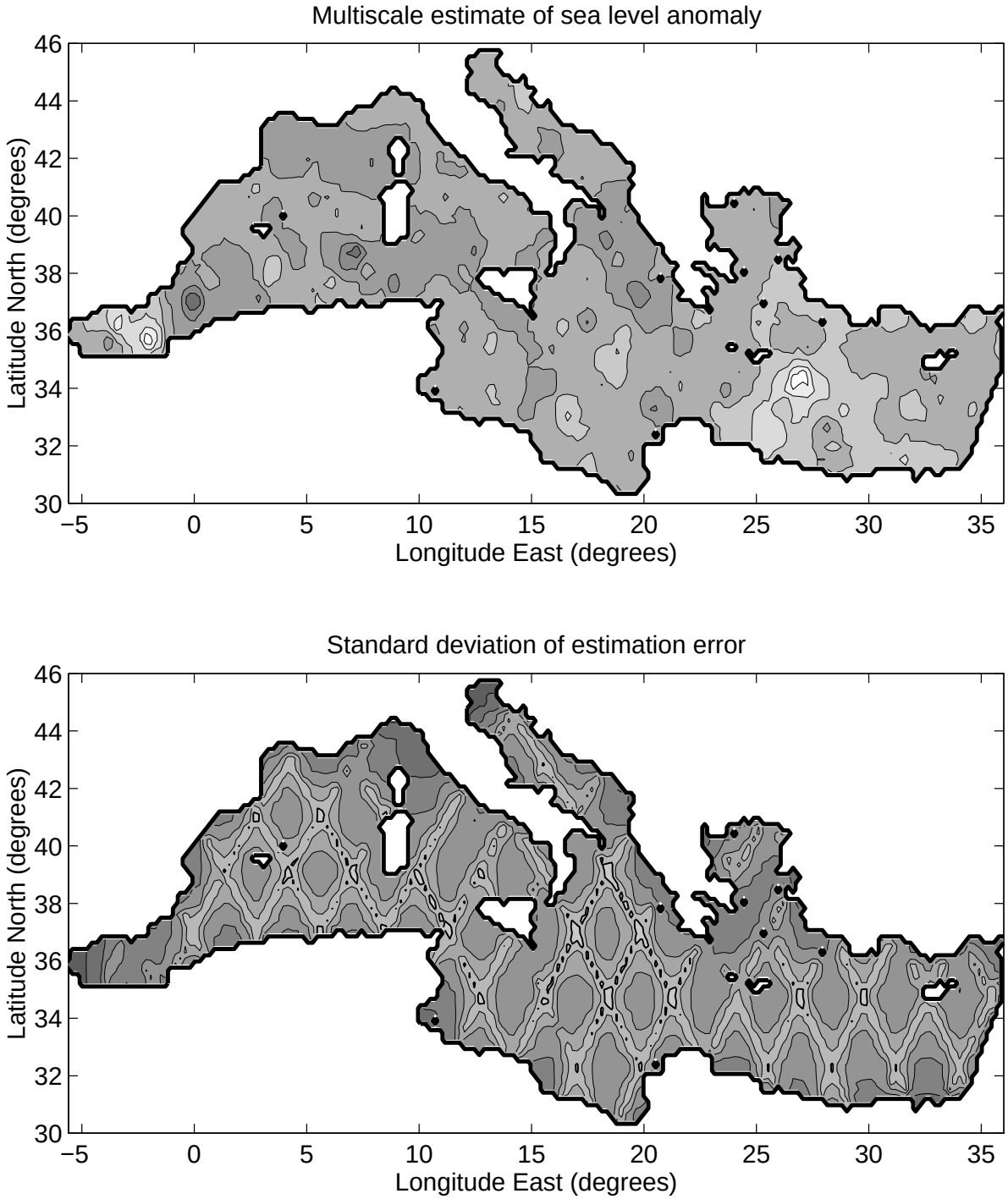

Figure 6. Multiscale estimates (top) and standard deviation of uncertainty (bottom) of sea level anomaly. The maps are based on the same 10-day TOPEX data as in Figs. 4 and 5, but this time a first-order polynomial model has been used to remove the correlated component of measurement error along each satellite track. Contour intervals are as in Fig. 5.

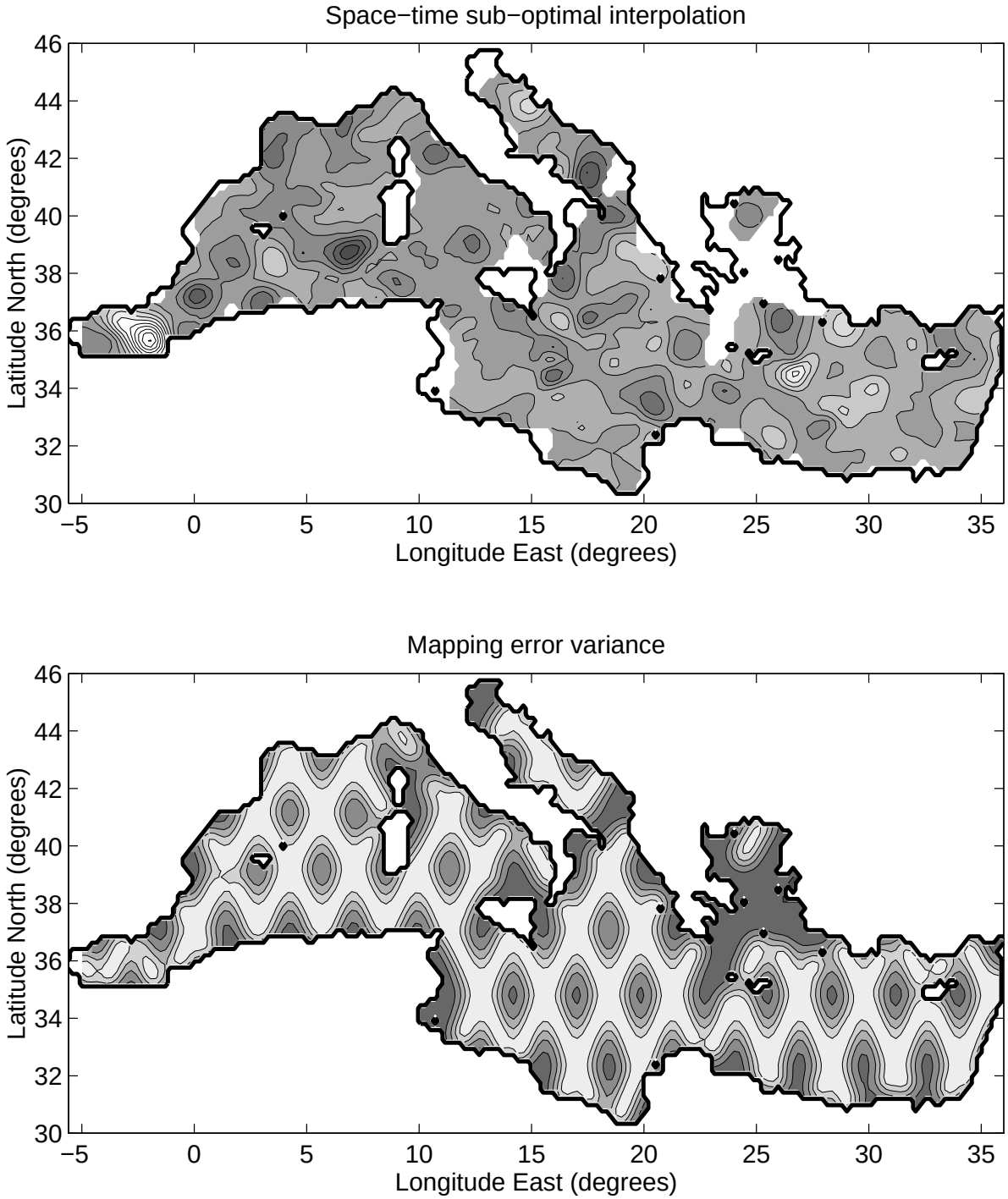

Figure 7. Maps of sea-level anomaly (top) and normalised mapping error variance as a percentage of the total signal variance (bottom) for a sub-optimal space time optimal interpolation scheme. The maps are based on the same 10-day TOPEX data as in Figs. 4, 5, and 6. Contour intervals are 3 cm for the estimates and 20% for the uncertainty. (Courtesy of Nadia Ayoub and Pierre De May.)

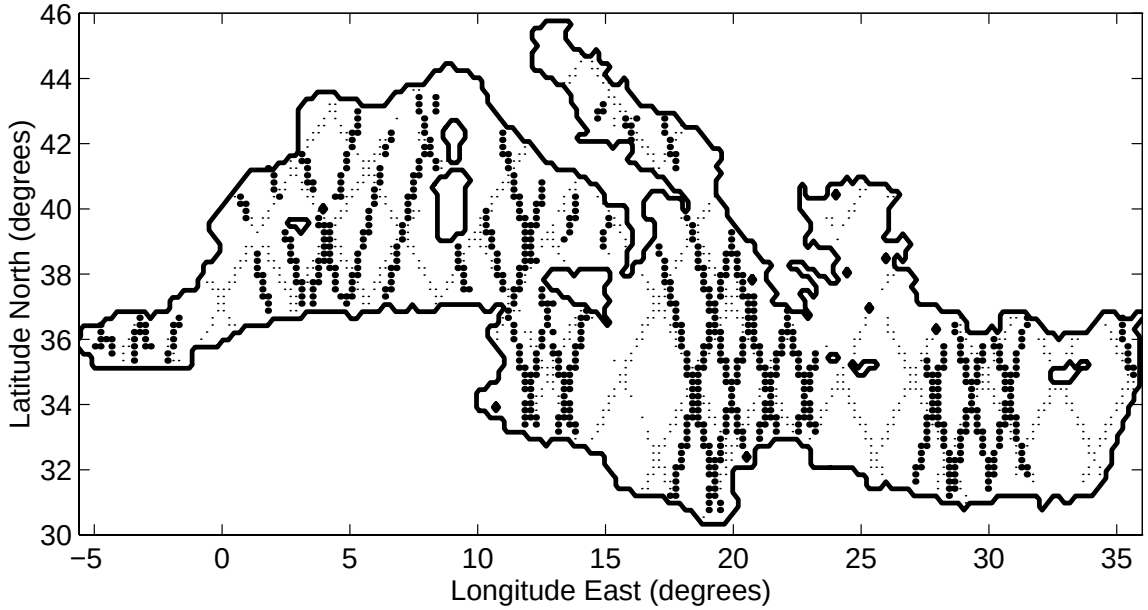

Figure 8. Additional coverage provided by the ERS-1 altimeter for the period May 9–19, 1993 (repeat cycle 24), concurrent with that of Figs. 4, 5, 6, and 7. The small dots indicate tracks of the TOPEX altimeter while the larger dots indicate ERS-1 tracks; the dots are shown gridded to the finest scale of the multiscale tree.

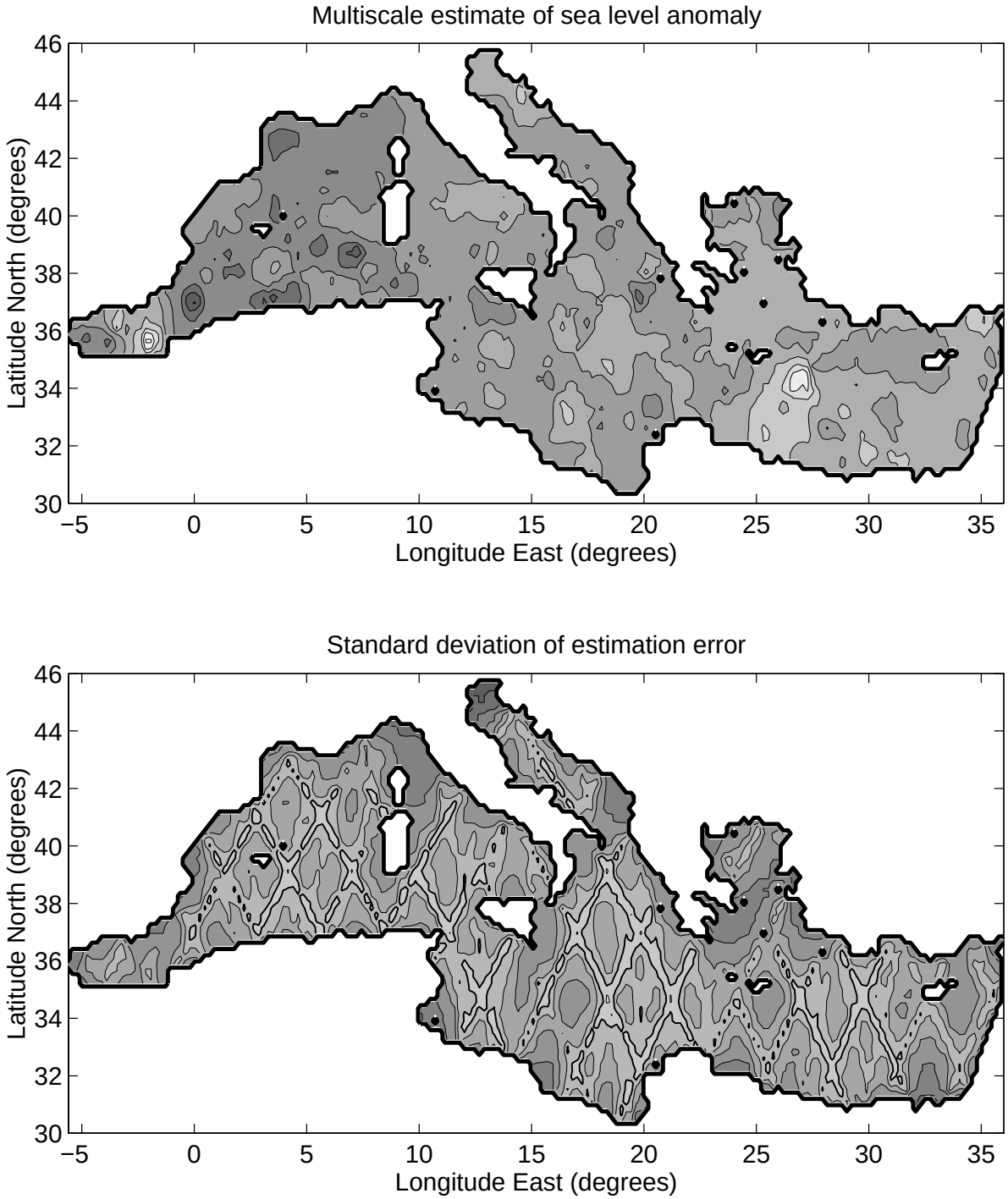

Figure 9. Multiscale estimates (top) and standard deviation of uncertainty (bottom) of sea level anomaly. The maps are computed from TOPEX and ERS-1 data using the same multiscale model as that used to create Fig. 6. Contour intervals are as in Figs. 5 and 6.